International Journal of Digital Earth

ISSN: 1753-8947 (Print) 1753-8955 (Online) Journal homepage: http://www.tandfonline.com/loi/tjde20

Spatial estimation of wind speed: a new integrative model using inverse distance weighting and power law

Emre Ozelkan, Gang Chen & Burak Berk Ustundag

To cite this article: Emre Ozelkan, Gang Chen & Burak Berk Ustundag (2016): Spatial estimation of wind speed: a new integrative model using inverse distance weighting and power law, International Journal of Digital Earth

To link to this article: http://dx.doi.org/10.1080/17538947.2015.1127437

Published online: 15 Jan 2016.

INTERNATIONAL JOURNAL OF DIGITAL EARTH, 2016
http://dx.doi.org/10.1080/17538947.2015.1127437

Taylor & Francis
Taylor & Francis Group

Spatial estimation of wind speed: a new integrative model using inverse distance weighting and power law

Emre Ozelkan[a,b,c], Gang Chen[b,c] and Burak Berk Ustundag[a]

[a]Agricultural & Environmental Informatics Research and Application Centre, Istanbul Technical University, Istanbul, Turkey; [b]Department of Geography and Earth Sciences, University of North Carolina at Charlotte, Charlotte, NC, USA; [c]Laboratory for Remote Sensing and Environmental Change (LRSEC), University of North Carolina at Charlotte, Charlotte, NC, USA

ABSTRACT

Spatial interpolation (SI) is currently one of the most common ways to estimate wind speed (Ws). However, classic SI models either ignore the complex geography [e.g. inverse distance weighting (IDW)], or demand high computational resources (e.g. cokriging). This study aimed to develop a simple yet effective SI model for estimating Ws in Eastern Thrace of Turkey. This new method, named $MIDW_{(Ws)}$, is a modified IDW through the integration of IDW with wind profile model, power law (PL), representing the influence of land cover and topography on Ws. Terrain features and elevation data of PL were obtained using normalized difference vegetation index (NDVI) and digital elevation model (DEM), respectively. Results showed superior and comparable performance of $MIDW_{(Ws)}$ to standard IDW and ordinary kriging (OK) across all months of year. Compared to ordinary cokriging (OCK) using DEM as covariate, $MIDW_{(Ws)}$ generated better results in the arid–semiarid seasons (around summer). Local complex atmospheric conditions during rainy seasons (around winter) may have affected the performance of incorporating PL with $MIDW_{(Ws)}$. Generally, the proposed $MIDW_{(Ws)}$ is simpler and easier to implement compared to OCK. For landscape-scale projects, its high computational efficiency and relatively robust performance show potential to deal with large volumes of datasets.

ARTICLE HISTORY
Received 10 August 2015
Accepted 29 November 2015

KEYWORDS
Wind speed; power law; NDVI; spatial interpolation; modified inverse distance weighting

1. Introduction

Wind speed (Ws) is a key climatic variable of digital earth, considerably used in a range of fields, such as climatology, oceanography, renewable energy, aerosol and pollutant transport, urbanization, agriculture, and disaster management (Morais et al. 2008; Curry, van der Kamp, and Monahan 2012; Yu et al. 2012; Vahidnia et al. 2013; Lorente-Plazas et al. 2014; Lorente-Plazas et al. 2015). The speed of wind has been discovered to be sensitive to the characteristics of local topography, surface roughness, and land cover among others, which often vary from region to region and are of high fluctuations, making the assessment of wind energy a challenging task (Curry, van der Kamp, and Monahan 2012; Philippopoulos and Deligiorgi 2012; Lorente-Plazas et al. 2014).

Spatial estimation of Ws mainly relies on spatial interpolation (SI), which generalizes Ws observations from a limited number of meteorological stations to the other locations with no prior Ws measurements (Luo, Taylor, and Parker 2008; Joyner et al. 2015; Mentis et al. 2015). Popular SI models include inverse distance weighting (IDW), kriging and cokriging (Apaydin, Sonmez, and Yildirim 2004; Cellura et al. 2008b; Joyner et al. 2015). While easy to comprehend and implement,

CONTACT Emre Ozelkan emreozelkan@itu.edu.tr

IDW typically demonstrates inferior performance compared to the more sophisticated geostatistical methods of kriging and cokriging (Apaydin, Sonmez, and Yildirim 2004; Luo, Taylor, and Parker 2008). Especially for cokriging, it has a unique feature of incorporating covariates [e.g. ancillary data of digital elevation model (DEM)] to estimate Ws. Cokriging constantly shows superior performance across topographies, although its computation is relatively intensive (Luo, Taylor, and Parker 2008; Joyner et al. 2015).

For a landscape-scale estimation of Ws, a dilemma is often caused by the desires to improve model accuracy while reducing the needs of computational resources (e.g. to lower processing costs and increase computation efficiencies). Hence, an important question needing to be addressed is whether the accurate spatial estimation of Ws can be achieved through an integration of a simple, yet effective SI model with valuable ancillary data (a strategy proven effective in cokriging) that can be easily and economically derived from Earth observation sensors. Based on the aforementioned classic SI models, one potential solution is to modify IDW, so it can incorporate covariates in Ws estimation. In order to achieve comparable or even superior performance to kriging and cokriging, such covariates should not only reflect the influence from topography (e.g. using DEM), but also represent other landscape characteristics that may influence the speed of wind (e.g. surface roughness and land cover). We noticed that all those factors are well simulated in wind profile models, such as the log-linear law (Log LL), logarithmic law (Log L) and power law (PL) (Patel 2006; Ozgonenel and Thomas 2012; Schallenberg-Rodriguez 2013). Among them, PL (also known as the exponential Hellmann law) is one of the most popular and useful due to its well-balanced simplicity and accuracy (Schallenberg-Rodriguez 2013; Sigal et al. 2015). Earth observation data (e.g. satellite imagery and products) with increased quality and decreased costs can be used to parameterize PL (Cellura et al. 2008a). Hence, our assumption was that the integration of IDW and PL can substantially improve the performance of the traditional IDW-based Ws estimation while retaining model simplicity.

The main objective of this research was to develop a novel SI model that can be efficiently used for landscape-scale, spatially explicit Ws estimation with satisfactory accuracies. Based on the idea of incorporating PL into IDW, the Ws estimation model was given a name modified IDW – $MIDW_{(Ws)}$. In this study, it was compared with standard IDW, and two popular geostatistical methods for SI of climate data – ordinary kriging (OK) and ordinary cokriging (OCK) (Apaydin, Sonmez, and Yildirim 2004; Luo, Taylor, and Parker 2008). Since Ws is a typical climatic variable with significant seasonal variations, we further analyzed the dynamics of model performance over all the 12 months of the year.

2. Data

2.1. Study area

The study area of Eastern Thrace is located in northwest Turkey between 26°0′ and 29°2′ eastern meridians and 40°0′ and 42°2′ northern parallels, covering an area of 23,764 km^2. The area is surrounded by the Black Sea in the north, the Aegean Sea in the west, and the Marmara Sea in the south. In the north, Strandzha (Star) Mountains are parallel to the Black Sea coast with its highest elevation over 1000 m. In the south, the Ganos and Koru Mountains are up to 945 m. Low hills cover the rest of the area (Thrace Development Agency 2015). According to the geographical conditions, three different regional climates, Continental, Black Sea, and Marmara, are prevalent over the area (Figure 1; Sensoy et al. 2008). The continental climate in Eastern Thrace has hot summers and cold winters; dry forests and steppes are the general natural vegetation (Turkish State Meteorological Service 2003; Sensoy et al. 2008). Marmara climate is a transition climate between Continental, Black Sea, and Mediterranean climates. Specifically, Marmara climate's winter is not as cold as the Continental and not as warm as the Mediterranean climate; and its summer is not as rainy as the Black Sea and not as dry as the Continental climate (Turkish State Meteorological Service 2003; Sensoy et al. 2008). Accordingly, the typical vegetation living in the Marmara climate is Mediterranean origin scrub at low altitudes, and Black Sea origin moist forests at the north-facing aspects of high

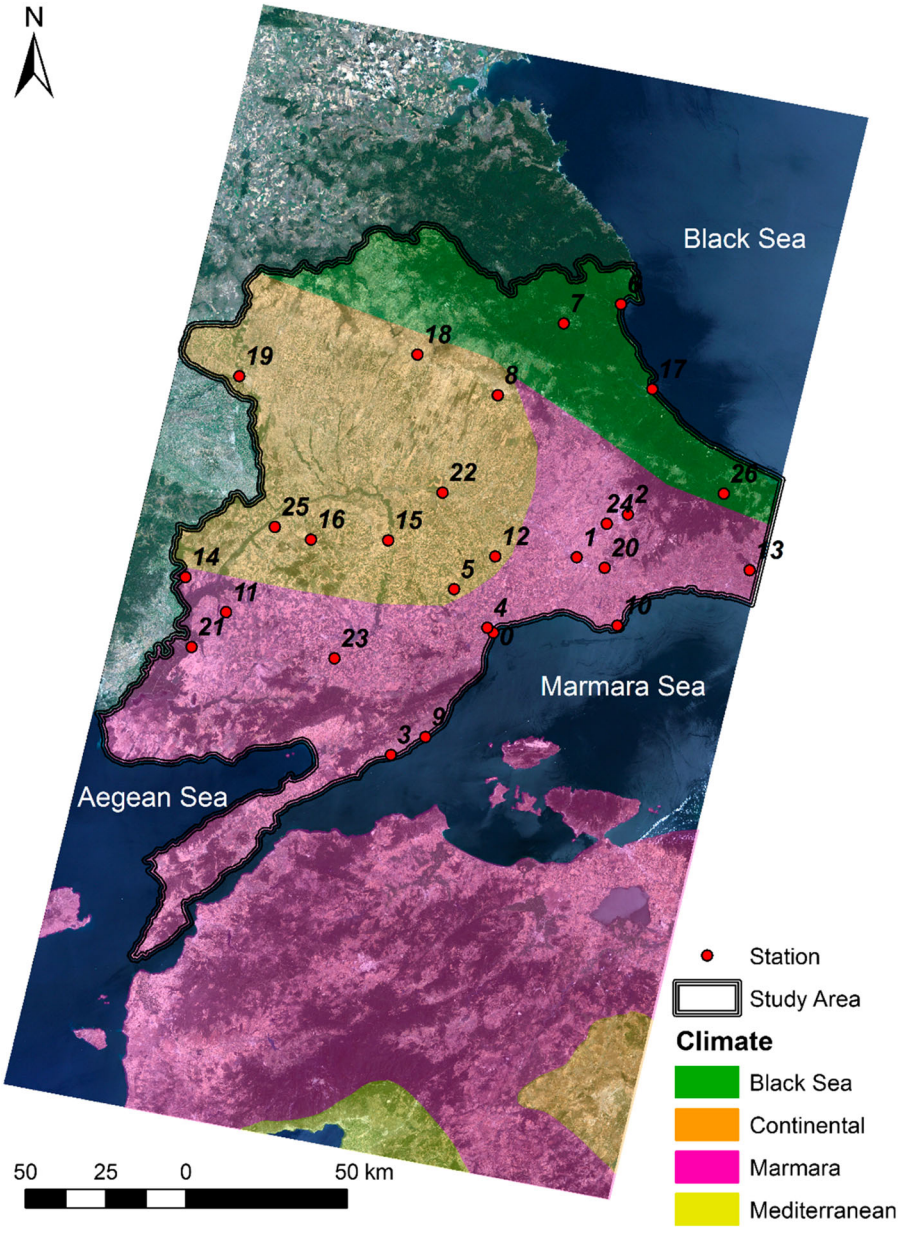

Figure 1. The region's climatic zones and the distribution of *in situ* climatological stations over a Landsat-5 TM true color (bands 3, 2, 1) image covering the Eastern Thrace region.
Source: Sensoy et al., 2008; Ozelkan et al., 2015.

altitudes (Turkish State Meteorological Service 2003; Sensoy et al. 2008). The Black Sea climate exists along the Black Sea coast of the study area and the northern aspects of the mountains. All seasons of the Black Sea climate are rainy and the seasonal variation of air temperature is low compared to the other climates; its natural vegetation is moist broadleaf forests in coastlines and coniferous forests at high elevations (Turkish State Meteorological Service 2003; Sensoy et al. 2008). The average, minimum, maximum, and standard deviation of four long-term climatic variables (i.e. Ta: air temperature, Pt: precipitation total, RH: relative humidity, and Ws) obtained by Turkish State Meteorological Service since 1970s in Eastern Thrace are presented in Table 1.

Table 1. The average, minimum, maximum, and standard deviation of long-term (between 1970 and 2014) climatic variables in Eastern Thrace (Ta: air temperature, Pt: precipitation total, RH: relative humidity, and Ws: wind speed).

	Ta (°C)	Pt (mm)	RH (%)	Ws (m/s)
Average	13.1	47.8	73.0	2.9
Minimum	2.2	5.2	55.8	1.0
Maximum	25.0	121.7	86.9	8.1
Standard deviation	7.1	21.4	7.0	1.5

2.2. Field data

Monthly Ws climate data acquired from 27 *in situ* climatological stations over the Eastern Thrace region of Turkey were used in this study (Figure 1). In fact, there were more stations in the region; however, not all of them consistently collected measurements over long terms. Only those having at least 10 years of Ws data were selected to reflect the climate. Although the time periods of measurements varies slightly across stations due to data availability, local climatic, and land-cover conditions did not experience major changes. The long-term annual average Ws values were 1.6 m/s, 2.8 m /s, and 5.0 m/s for the Continental, Marmara, and Black Sea climates, respectively. The minimum and maximum monthly average values observed in the study area were 1.0 m/s and 8.1 m/s, respectively, with a standard deviation of 1.5 m/s.

2.3. Remote sensing data and pre-processing

The study area corresponds to the extent of two Landsat images scenes (path/row: 181/31 and 32). A total number of 432 Landsat-5 (TM) and Landsat-7 (ETM +) NDVI images over the study area were acquired between January 2000 and January 2012 from the United States Geological Survey (USGS) data portal. All the Landsat surface reflectance images were obtained at a 30 m spatial resolution, and have been atmospherically and geometrically corrected by NASA. A remote sensing vegetation index, NDVI (Normalized Difference Vegetation), was used to express terrain features in PL and was calculated as follows:

$$\mathrm{NDVI} = (\lambda_{\mathrm{NIR}} - \lambda_{\mathrm{RED}})/(\lambda_{\mathrm{NIR}} + \lambda_{\mathrm{RED}}), \quad (1)$$

where λ_{RED} is the red and λ_{NIR} is the near infrared spectral reflectance. NDVI not only represents the abundance of live vegetation on earth surface, but can also be linked to the surface roughness of varying types of land-cover classes (Liu, Stanturf, and Goodrick 2010; Lee and Kim 2012; Bae and Ryu 2015; Walker, de Beurs, and Henebry 2015). Such features can contribute to the calculation of Ws and will be described in detail in Section 3.3. To be consistent with the monthly *in situ* Ws measurements, monthly NDVI images were generated by averaging NDVI images of the same months. To reduce spectral noises, NDVI images were smoothed using a mean filter with a small kernel of 3×3 pixels. Larger kernels (e.g. $> 3 \times 3$ pixels) were not utilized because they dramatically reduced the variation of NDVI values in our tests. An example of a July NDVI map is presented in Figure 2.

DEM over the same area was acquired directly from the ASTER Global Digital Elevation Model (ASTER GDEM) that has a 30 m spatial resolution (NASA 2015), the same as the resolution of NDVI imagery used in this study (Figure 2). DEM was used to extract altitude values, with more details described in Section 3.3.

3. Methodology

In this section, we present the basic principles of IDW, OK, and OCK, as well as a detailed description of the proposed $\mathrm{MIDW}_{(\mathrm{Ws})}$ model, an integration of the standard IDW and a wind profile model PL. For each of the four types of models, we analyzed the impact of seasonal variation on model performance through comparing the model results across all the 12 months of the year. Because NDVI

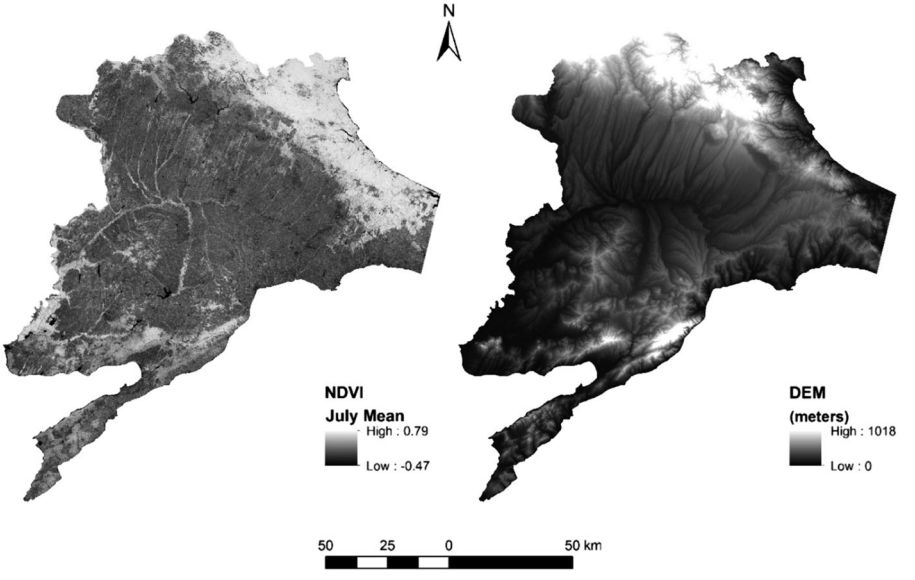

Figure 2. An example of remote sensing products, NDVI and DEM, used in this study.
Source: USGS 2014; NASA 2015.

was utilized in $MIDW_{(Ws)}$, and it varied with the seasonal change of vegetation phenology and land cover (e.g. snow cover in winter), we further evaluated the performance of $MIDW_{(Ws)}$ in two scenarios: (i) using NDVI to assist in estimating Ws of the corresponding month, and (ii) applying NDVI from only one of the 12 months to consistently estimate Ws across the year. The reason for such testing was due to the fact that seasonal climatic variation (e.g. harsh weather conditions with frequent precipitation especially in wet season between mid of autumn and mid of spring) may change the role or quality of NDVI in Ws estimation. So, using NDVI from one single season with stable atmospheric conditions may be a better way to characterize terrain features.

3.1. Inverse distance weighting

As a deterministic SI method, IDW is based upon the principle that the value of estimated point is more correlated with the value of a closer known point than a far one (Tobler 1970; Apaydin, Sonmez, and Yildirim 2004). The influence of known point declines by increasing distance between the estimated and known points, and such influence is defined as weight that is accepted as inversely proportional to the square of the distance (Hartkamp et al. 1999). The IDW equation is given as follows.

$$\hat{Z}(u_0) = \frac{\sum_{i=1}^{N} Z(u_i) w_i}{\sum_{i=1}^{N} w_i} \tag{2}$$

with $i = 1, \ldots, N$ and $w_i = d_{0,i}^{-p}, \ i = 1, \ldots N$.

where u_0 is the location of an estimated point, and $u_i (i = 1, \ldots N)$ are the locations of known points (i.e. field measurements). The estimated value $\hat{Z}(u_0)$ is the weighted average of N measured values $Z(u_i)$. The weight or influence of each known data is calculated as $w_i = d_{0,i}^{-p}$, where w is weight, d is the Euclidian distance between the estimated and the known points (i), and p is exponential power parameter. Lloyd (2005) found that if the value of the p increases, the estimation result becomes more similar to the value of the closest known point. Thus, p is usually set to 2, which was also used in our study.

3.2. Ordinary kriging and cokriging

As a geostatistical SI method, kriging is similar to IDW in a way that they derive unknown values through calculating the weighted mean of measured/known values (Lloyd 2005). However, during the weight computation, kriging considers not only the distance, but also the spatial distribution of the measurement points that contain spatial autocorrelation (Johnston et al. 2001). All types of kriging are deemed as basic linear regression estimators (Mutua and Kuria 2012). They differ from each other in the assessment of mean values (i.e. trend component). For example, OK assumes that the mean values of known and estimated points are equal and constant in the local neighborhood of each estimated point (Garška and Krūminiene 2004). A typical equation of OK is given as follows:

$$\hat{Z}(u_0) = \sum_{i=1}^{N} \lambda_i^{OK}(u) Z(u_i) \quad \text{with} \quad \sum_{i=1}^{N} \lambda_i^{OK}(u) = 1, \tag{3}$$

where λ_i are the weights assigned to known values $Z(u_i)$ such that their total is 1 and the computed weights minimize the estimation variance $\sigma_E^2(u) = \mathrm{Var}\{\hat{Z}(u_0) - Z(u_i)\}$ under the unbiasedness constraint of the estimator $E\{\hat{Z}(u_0) - Z(u_i)\} = 0$ (Goovaerts 2000).

An empirical semivariogram model is often built to obtain the variance of weights (λ_i) in different distances to solve Equation (4) (Luo, Taylor, and Parker 2008).

$$\gamma_{i,j} = 0.5E[(Z(u_i) - Z(u_j))^2], \tag{4}$$

where $\gamma_{i,j}$ is the semivariance between data points i and j. Here, we used the typical spherical semivariogram model. For detailed information about kriging and semivariogram models, the readers may refer to Goovaerts (2000); Sertel, Kaya, and Curran (2007); Wang, Li, and Christakos (2009).

Cokriging is a multivariate version of kriging, which uses information from additional covariates (i.e. ancillary data) to assist in model estimation (Goovaerts 2000). Cokriging regards the spatial cross autocorrelation between primary and secondary/ancillary variables to improve model accuracy, and it is typically utilized when the distribution or the number of primary variable recording locations (i.e. Ws for this study) is insufficient (Zhang, Li, and Travis 2009). OCK was tested in this study using DEM as a secondary variable.

$$\hat{Z}(u_0) = \sum_{i_1=1}^{N_1} \lambda_{i_1}^{\mathrm{OCK}}(u) Z(u_{i_1}) + \sum_{i_2=1}^{N_2} \lambda_{i_2}^{\mathrm{OCK}}(u) Z(u_{i_2}), \quad \text{with} \quad \sum_{i_1=1}^{N_1} \lambda_{i_1}^{\mathrm{OCK}}(u) = 1, \quad \text{and} \quad \sum_{i_2=1}^{N_2} \lambda_{i_2}^{\mathrm{OCK}}(u) = 0, \tag{5}$$

Both OK and OCK were performed in ArcGIS (Redlands, CA, USA). For parameterizing semivariogram, the trial and error method was used to manually determine the best parameters (leading to lowest model errors): lag = 14.82 km, number of lags = 12, nugget = 1.24 $(\mathrm{m/s})^2$, partial sill = 0.97 $(\mathrm{m/s})^2$, and range = 110.42 km.

3.3. Modified inverse distance weighting ($MIDW_{(Ws)}$)

Observations of Ws at climate stations reflect varying characteristics of local topography, surface roughness and land cover. To estimate an unknown Ws of a specific point, all the observation data should be normalized by taking into account those effects before the interpolation process

can be accurately conducted in SI. Hence, the first step of $MIDW_{(Ws)}$ was the normalization of all the known Ws (at 27 stations for our study) through the use of a wind profile model PL. Simple yet useful PL expresses the vertical wind variation according to the difference between estimated and reference Ws in altitude, surface roughness, and land cover (Sahin 2004; Schallenberg-Rodriguez 2013; Sigal et al. 2015). The formula of PL is given as follows.

$$\mathrm{Ws(est)} = \mathrm{Ws(ref)} \times \left(\frac{h(\mathrm{est})}{h(\mathrm{ref})}\right)^{\alpha}, \tag{6}$$

where Ws(est) and Ws(ref) are the Ws of estimated and reference (i.e. known measured stations data) points, respectively; h(est) and h(ref) are the altitude of estimated and reference points, respectively; and α is Hellman coefficient signifying surface roughness and land-cover types. In $MIDW_{(Ws)}$, PL was fed by DEM and NDVI to derive h and α, respectively. Specifically, h was directly transferred to PL from DEM. NDVI values were manually matched to popular α values presented by Patel (2006) (Table 2). To be sure about matching, NDVI values were examined all over the study area by considering all terrain types mentioned by Hellman.

The second step of $MIDW_{(Ws)}$ was to integrate the normalized Ws with IDW. Specifically, all the normalized Ws observations were used to replace the original known point data measured at reference stations, and were fed to the standard IDW formula. The formula of $MIDW_{(Ws)}$ is given as follows.

$$\mathrm{Ws}(u_0) = \frac{\sum_{i=1}^{N} \mathrm{Ws}(u_{0,i})\, w_i}{\sum_{i=1}^{N} w_i} \tag{7}$$

$$\text{with } \mathrm{Ws}(u_{0,i}) = \mathrm{Ws}(u_i) \times \left(\frac{h(u_0)}{h(u_i)}\right)^{\alpha},\ i = 1, \ldots, N \text{ and } w_i = d_{0,i}^{-p},\ i = 1, \ldots N.$$

where u_0 and u_i are the locations of estimated ($\mathrm{Ws}(u_{0,i})$) and known Ws, respectively. $\mathrm{Ws}(u_{0,i})$ is the result of PL that uses known/reference data $\mathrm{Ws}(u_i)$, estimated and reference points' h values as $h(u_0)$ and $h(u_i)$, respectively. Similar to the standard IDW, the weight or influence of each known point was calculated as $w_i = d_{0,i}^{-p}$, where w represented weight, d was Euclidian distance, and p was set to 2. A simple computation example to illustrate the principle of the developed $MIDW_{(Ws)}$ is presented in Figure 3. In this example, Ws, h, and NDVI values were available for the three sample reference stations ($N = 3$) within three image pixels. The corresponding α values of NDVI can be found in Table 2. The distances between the reference and the estimated pixels were $d_{0,1}$ (3000 m), $d_{0,2}$ (5000 m), and $d_{0,3}$ (5000 m), respectively. Following Equation (7), the computation for estimating an unknown Ws is illustrated in Figure 3.

3.4. Model calibration and validation

Among all the *in situ* measurements collected from the 27 stations, Ws data from 21 stations (78% of the data) were used for model calibration, and the remainder was used for validation. Both calibration and validation stations were selected on the basis that they both reflected the three main types of regional climate in the study area. The performance of models was compared using three

Table 2. Land-cover classes, Hellman coefficient (α) values (Patel 2006), and the corresponding NDVI values.

Terrain Type	α	NDVI
Lakes, ocean, and smooth hard ground	0.10	−1.000–0.000
Foot-high grass on level ground	0.15	0.251–0.300
Tall crops, hedges, and shrubs	0.20	0.301–0.600
Wooded country with many trees	0.25	0.601–1.000
Small town with some trees and shrubs	0.30	0.201–0.250
City area with tall buildings	0.40	0.001–0.200

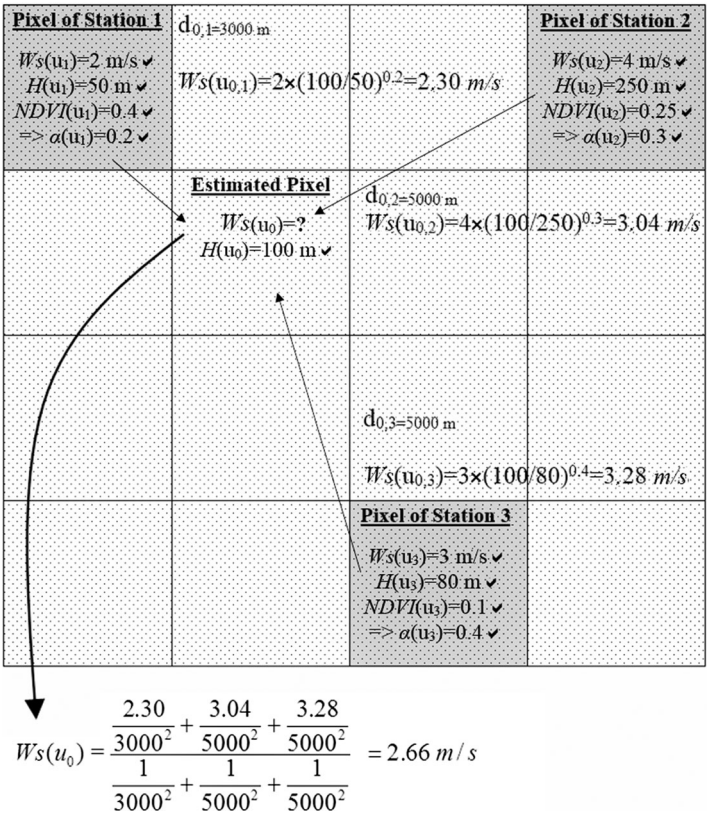

Figure 3. The illustration of $MIDW_{(Ws)}$ computation. The gray pixels overlap the *in situ* climate stations and the others express estimated pixels. A representative computation is presented for a sample pixel.

criteria of root mean square error (RMSE), Pearson's correlation coefficient (r), and significance F (SF, significance probability of ANOVA) that were generated using the validation data, accounting for 22% of all the data.

4. Results and discussion

4.1. Influence of monthly NDVI on $MIDW_{(Ws)}$

A total of 156 $MIDW_{(Ws)}$ models were developed for the two scenarios described at the beginning of Section 3, i.e. using the same month of NDVI for estimating Ws, and applying only one month of NDVI to consistently estimate Ws across the year. Through comparisons of the modeling results, July NDVI was discovered to be the best to use, because its corresponding models outperformed all the other ones in most cases, i.e. 9 of the 12 months (Figure 4). We also found that using NDVI acquired in or near summer (e.g. May, June, and August) improved the performance of $MIDW_{(Ws)}$ than those using NDVI collected close to winter (Figure 4). The highest model errors were generated with December NDVI that had the highest precipitation and cloudiness with lowest insolation for our study area (Ozelkan et al. 2015). The distribution and number of NDVI images, long-term monthly average rainy days, and long-term daily average insolation hours for each month of study are shown in Figure 5. In addition, monthly NDVI in Figure 4 refers to the aforementioned first scenario described at the beginning of Section 3. While the corresponding models' performance were superior to many others developed for the second scenario, they were not as good as the

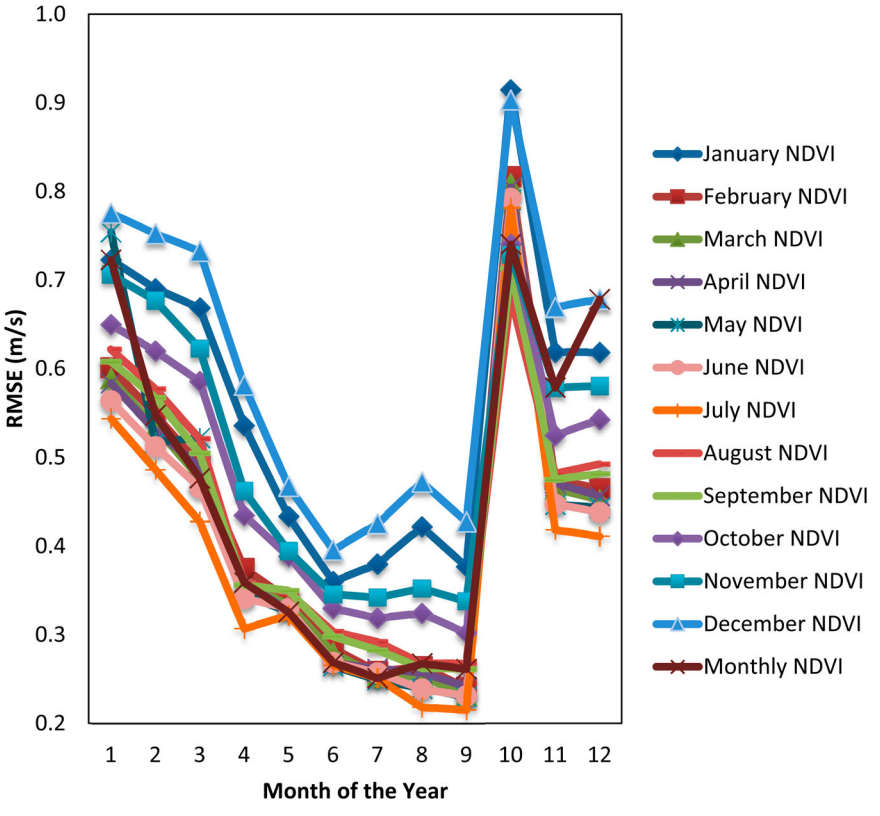

Figure 4. The values of root mean square error (RMSE) values derived from $MIDW_{(Ws)}$ using NDVI of various months. Monthly NDVI refers to the NDVI values calculated in the same month as shown on the *x* axis.

$MIDW_{(Ws)}$ models using July NDVI as an input, with a larger error of 0.47 m/s on average across the year.

Theoretically, it is more reasonable to use NDVI to represent terrain surface conditions of the corresponding months and estimate Ws (i.e. scenario one). However, our results were not consistent

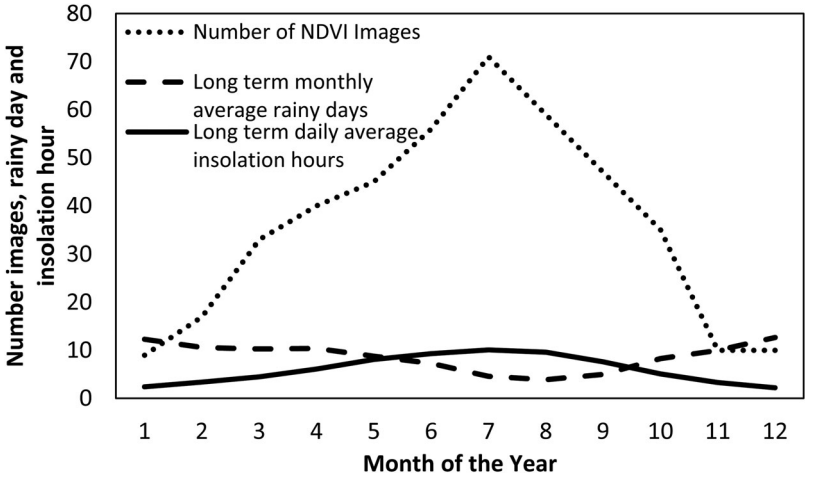

Figure 5. The distribution of number of NDV images, long-term monthly average rainy days, and long-term daily average insolation hours for each month.

with such an assumption. Potential reasons may include: (i) the study area of Eastern Thrace is surrounded by the Black Sea, the Aegean Sea, and the Marmara Sea (Figure 1). The high moisture in winter and early spring often causes fog and haze (UMBC 2015). Although all the remotely sensed data have been atmospherically corrected, local complex atmospheric distortions may not be completely removed. Hence, NDVI values possibly contained errors; (ii) the conversion Table 2 is basically an experience model linking land-cover types and NDVI. However, the frequent precipitation in or near winter could reduce the heterogeneity of the local terrestrial surface. While land cover may not change, NDVI values have been influenced by climate. Hence, Hellman coefficients may not be accurately derived.

4.2. Comparison among IDW, OK, OCK, and MIDW$_{(Ws)}$

According to the derived RMSEs (Table 3), MIDW$_{(Ws)}$ was better than IDW for nine months (between April and December), and for the rest the error of MIDW$_{(Ws)}$ was slighter higher with an average difference of 0.02 m/s. The performance of MIDW$_{(Ws)}$ was found to be superior to OK in all cases. Compared to OCK fed with DEM, MIDW$_{(Ws)}$ generated better results in five months (May, June, July, August, and September). For the rest of the year (except October), the results from MIDW$_{(Ws)}$ and OCK were actually similar with an average difference of 0.06 m/s. Overall, the monthly best results were either produced by OCK or MIDW$_{(Ws)}$. According to r and SF (Figure 6), MIDW$_{(Ws)}$ generated more correlated results than the others for six months (May to October). For the rest of the year, OCK had superior performance. In the months when MIDW$_{(Ws)}$ generated more correlated results, r and SF values were better than OCK with an average difference of 0.16 and 0.14, respectively. On the other hand, in the months when OCK generated more correlated results, r and SF values were better than MIDW$_{(Ws)}$ with an average difference of 0.13 and 0.08, respectively. These show that in general MIDW$_{(Ws)}$ generated more robust and correlated results than OCK. For MIDW$_{(Ws)}$, the best result was generated for August with $r = 0.94$ and $SF = 0.01$ (99% confidence level). IDW and OCK produced most correlated results in March, with $r = 0.86$ and 0.91 and $SF = 0.03$ and 0.01 (97% and 99% confidence level), respectively. OK performed the best in August with $r = 0.87$ and $SF = 0.03$ (97% confidence level).

In general, the results in Figures 4 and 6 suggest that MIDW$_{(Ws)}$ and OCK are better options for Ws estimation in our study area, these were followed by the use of IDW and OK. Compared to OCK, MIDW$_{(Ws)}$ generated more accurate results in arid and semiarid seasons (around summer), while OCK was better around the rainy seasons (around winter). As previously discussed in Section 4.1, fog and haze in winter and spring (e.g. November to April) possibly reduced the quality of the remotely sensed NDVI data. Meantime, because the atmospheric events (e.g. precipitation) are more frequent and stronger than those in other seasons, it is also possible that the texture and pattern of

Table 3. Monthly root mean square error (RMSE) values for Ws estimation from MIDW$_{(Ws)}$, IDW, OCK, and OK.

	RMSE (m/s)			
Month	MIDW$_{(Ws)}$	IDW	OCK	OK
1	0.54	0.52	**0.46**	0.61
2	0.49	0.48	**0.43**	0.58
3	0.43	0.41	**0.32**	0.56
4	0.31	0.48	**0.30**	0.45
5	**0.32**	0.54	0.35	0.53
6	**0.27**	0.47	0.37	0.46
7	**0.25**	0.50	0.36	0.52
8	**0.22**	0.37	0.28	0.36
9	**0.22**	0.52	0.29	0.53
10	0.78	0.91	**0.35**	0.99
11	0.42	0.43	**0.36**	0.48
12	0.41	0.46	**0.35**	0.59

Note: Numbers bold and underlined represent the lowest RMSE for each month.

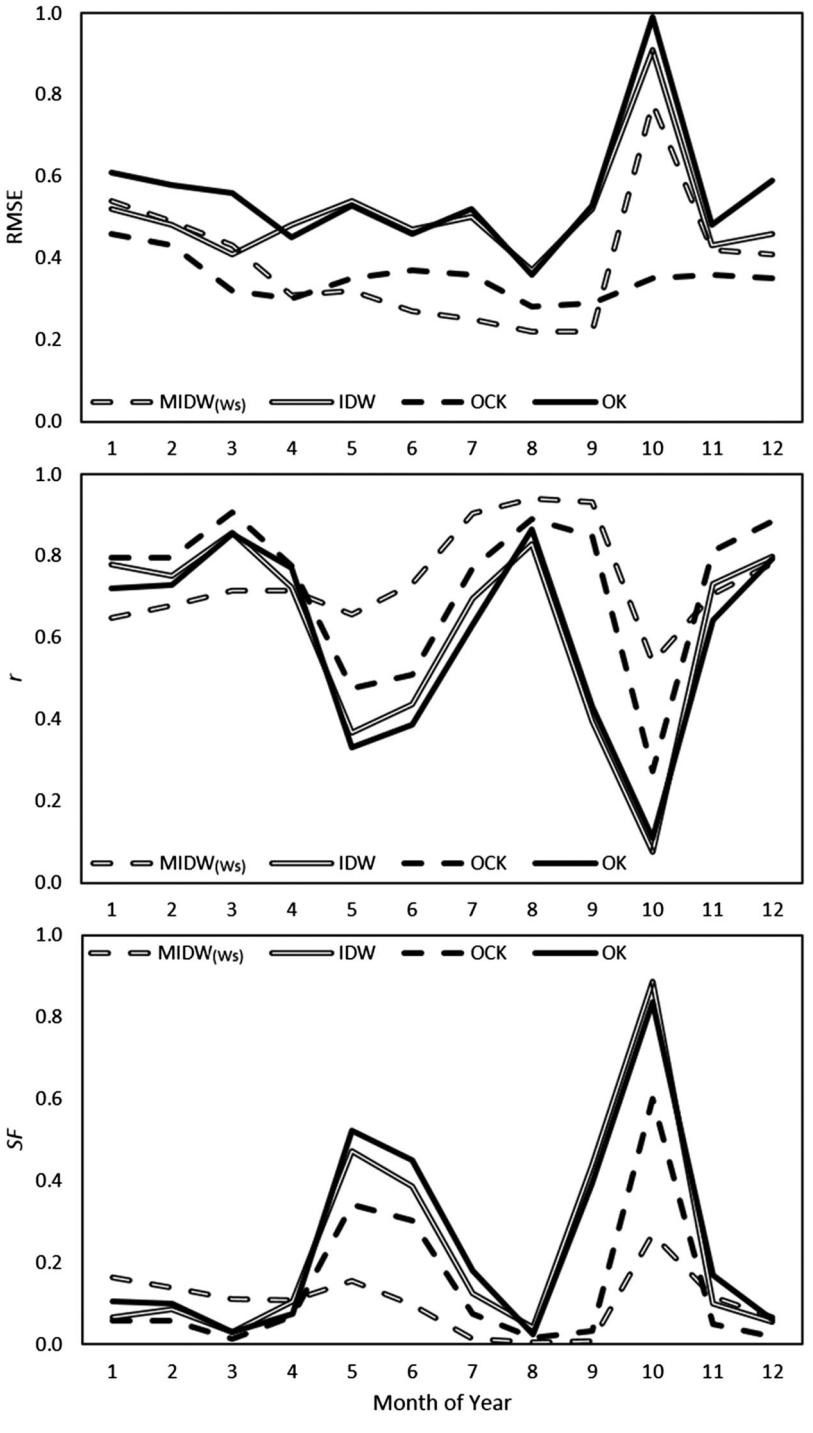

Figure 6. The distribution of root mean square error (RMSE), Pearson's correlation coefficient (*r*), and significance *F* (*SF*) values between known and estimated Ws using $MIDW_{(Ws)}$, IDW, OK, and OCK for each month of the year.

terrestrial surfaces are of high fluctuations from time to time, leading to high variations in NDVI over the same areas. In contrast, arid and semiarid seasons (e.g. May to September) allowed the heterogeneity of nature to be better observed by satellite sensors (Ji and Peters 2003; Gopinath et al.,

forthcoming). Consequently, NDVI played a more apparent role in Ws estimation using $MIDW_{(Ws)}$ that outperforms OCK in arid and semiarid season but not in others. Sample Ws maps generated using $MIDW_{(Ws)}$, IDW, OK, and OCK are presented in Figure 7. Clearly, the results from OK and IDW lacked spatial variation, and the maps of all methods contained a Bull's Eye effect in different ratios, which refers to unnatural neighboring zones around meteorological stations (Johnston et al. 2001). In other words, $MIDW_{(Ws)}$ and OCK allow fine-scale pixel by pixel examination of the study area by using ancillary remote sensing data. While the OCK map contained higher variation with the use of DEM, boundaries of zones were not as natural as those on the $MIDW_{(Ws)}$ map, due to the integrative use of land surface characteristics (i.e. NDVI and DEM). Those are important, because our study area is complex both in land cover with cities, agriculture lands, forests, etc. and in topography from the sea level to an altitude higher than 1000 m.

We noticed that OCK slightly outperformed $MIDW_{(Ws)}$ for most winter and spring seasons. However, OCK calculated variograms led to an intensive computation overhead, but our model integrates simple IDW and the PL theory dramatically improved the computational efficiency.

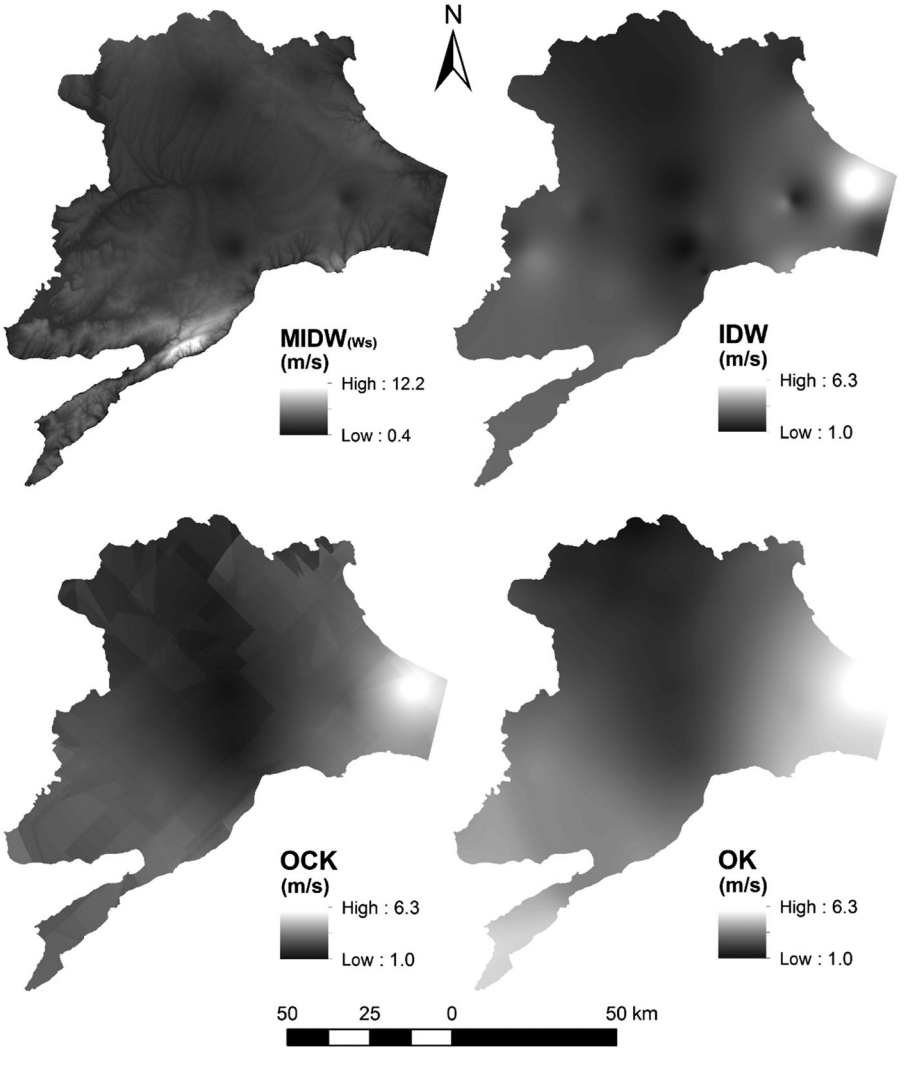

Figure 7. A sample of Ws spatial interpolation maps of $MIDW_{(Ws)}$, IDW, OCK, and OK for July.

For large-scale projects, $MIDW_{(Ws)}$ would be a viable solution for estimating Ws, if the computational resources are limited with short time frames. Even if those limitations do not exist, $MIDW_{(Ws)}$ possibly remains the best solution among IDW, OK, and OCK for most summer and fall seasons (i.e. arid and semiarid seasons) according to this study. Another fact that needs to be aware of is that, classic SI methods produce values within a controlled range (i.e. with upper and lower limits) assigned by interpolated dataset's minimum and maximum values or the variogram's (Ozelkan et al. 2015). The integration of PL with SI can generate estimates with an unrestricted range (see example in Figure 7) that may help to obtain real and microclimate values.

According to Wang et al. (2012), the accuracy of a SI is affected by the property of target, sampling scheme, and estimator (i.e. the procedure used to calculate an estimate). In our study, the emphasis was the comparison of SI methods (i.e. estimators). We also noted that local climate and land surface characteristics (i.e. the property of target) may have affected the results via influencing the estimation of NDVI. We did not discuss about the sampling scheme, because all the field stations have been set up following a random sampling strategy and cannot be changed.

Finally, while the application of land cover facilitated the estimation of Ws, the use of NDVI may not be the best way to represent landscape conditions due to severe weather events and the complex land surface structures. Future research will incorporate one or more remote sensing variables to better represent landscape conditions while mitigating the impact of atmospheric events.

5. Conclusion

This study proposed a new and simple SI method for spatial estimation of Ws, $MIDW_{(Ws)}$, which is IDW integrated with wind power law using NDVI and DEM to represent land use, surface roughness, and elevation. The eastern Thrace of Turkey that has complex geography was used as a case study area to evaluate our proposed model and several other popular ones, including IDW, OK, and OCK. The main findings of our study are listed as follows.

- Through the comparison of $MIDW_{(Ws)}$ results across the year, a consistent application of July NDVI was found to achieve higher accuracies than using NDVI of individual months.
- $MIDW_{(Ws)}$ results were significantly better than those of IDW in semiarid and arid seasons, and they were comparable to each other in the rainy seasons.
- $MIDW_{(Ws)}$ was found to have superior performance to OK across all the tested 12 months of the year.
- $MIDW_{(Ws)}$ generated better results in the arid and semiarid seasons (around summer), while OCK was better in the rainy seasons (around winter). Local complex atmospheric conditions during rainy seasons may have affected the performance of incorporating NDVI in $MIDW_{(Ws)}$ for Ws estimation.
- Although the model errors of $MIDW_{(Ws)}$ for the rainy season Ws estimation were higher than that of OCK (e.g. 0.04 m/s on average), $MIDW_{(Ws)}$ is simpler and easier to implement compared to OCK. Its advantages of high computational efficiency for big data processing can benefit large-scale Ws estimation.
- In contrast to the classic SI methods, $MIDW_{(Ws)}$ can produce estimates with an unrestricted range that may allow a more accurate estimation of Ws in areas of complex land cover and topography.

The results show that the simple but effective proposed SI method $MIDW_{(Ws)}$ can be a good and allowed alternative treatment for climatology, oceanography, renewable energy, aerosol and pollutant transport, urbanization, agriculture, disaster management, and may other fields of digital earth that interact with wind speed. Hence, the proposed method facilitates efficient and accurate management of the digital information of the Earth (Vahidnia et al. 2013), as well as the multidisciplinary collaboration between Earth, space, and information sciences to analyze natural and human sources phenomena (ISDE 2015).

Acknowledgements

The authors would like to thank the Turkish State Meteorological Service for the meteorological data. Special thanks to the General Directorate of Agricultural and Policy Tekirdağ Viticultural Research Station and the ADASTA Agricultural Products Food Industry and Trade Company for providing meteorological data of stations #4 and #5, respectively. The authors would like to thank Dr Cankut Ormeci, Dr Ertunga Cem Ozelkan, Serdar Bagis and Meric Yucel for data processing support and valuable suggestions. Dr Gang Chen gratefully acknowledges the support from the University of North Carolina at Charlotte through the Junior Faculty Development Award.

Disclosure statement

No potential conflict of interest was reported by the authors.

References

Apaydin, H., F. K. Sonmez, and Y. E. Yildirim.2004. "Spatial Interpolation Techniques for Climate Data in the Gap Region in Turkey." *Climate Research* 28: 31–40. doi:10.3354/cr028031.

Bae, J., and Y. Ryu. 2015. "Land Use and Land Cover Changes Explain Spatial and Temporal Variations of the Soil Organic Carbon Stocks in a Constructed Urban Park." *Landscape and Urban Planning* 136: 57–67. doi:10.1016/j.landurbplan.2014.11.015.

Cellura, M., G. Cirrincione, A. Marvuglia, and A. Miraoui. 2008a. "Wind Speed Spatial Estimation for Energy Planning in Sicily: Introduction and Statistical Analysis." *Renewable Energy* 33 (6): 1237–1250. doi:10.1016/j.renene.2007.08.012.

Cellura, M., G. Cirrincione, A. Marvuglia, and A. Miraoui. 2008b. "Wind Speed Spatial Estimation for Energy Planning in Sicily: A Neural Kriging Application." *Renewable Energy* 33 (6): 1251–1266. doi:10.1016/j.renene.2007.08.013.

Curry, C. L., D. van der Kamp, and A. H. Monahan. 2012. "Statistical Downscaling of Historical Monthly Mean Winds over a Coastal Region of Complex Terrain. I. Predicting Wind Speed." *Climate Dynamics* 38 (7–8): 1281–1299. doi:10.1007/s00382-011-1173-3.

Garška, R., and I. Krūminiene. 2004. "Spatial Analysis and Prediction of Curonian Lagoon Data with Gstat." *Mathematical Modelling and Analysis* 9 (1): 39–50. doi:10.1080/13926292.2004.9637240.

Goovaerts, P. 2000. "Geostatistical Approaches for Incorporating Elevation into the Spatial Interpolation of Rainfall." *Journal of Hydrology* 228 (1–2): 113–129. doi:10.1016/S0022-1694(00)00144-X.

Gopinath, G., G. K. Ambili, S. J. Gregory, and C. K. Anusha. Forthcoming. "Drought Risk Mapping of South-Western State in the Indian Peninsula – A Web Based Application." *Journal of Environmental Management*. doi:10.1016/j.jenvman.2014.12.040.

Hartkamp, A. D., K. De Beurs, A. Stein, and J. W. White.1999. *Interpolation Techniques for Climate Variables*. NRG-GIS Series 99-01. Mexico, DF: CIMMYT.

ISDE (International Society for Digital Earth). 2015. "About ISDE". Accessed 23 October 2015. http://www.digitalearth-isde.org/.

Ji, L., and A. J. Peters. 2003. "Assessing Vegetation Response to Drought in the Northern Great Plains using Vegetation and Drought Indices." *Remote Sensing of Environment* 87 (1): 85–98. doi:10.1016/S0034-4257(03)00174-3.

Johnston, K., J. M. Ver Hoef, K. Krivoruchko, and N. Lucas. 2001. *Using ArcGIS Geostatistical Analyst*. Redlands, CA: ESRI.

Joyner, T. A., C. J. Friedland, R. V. Rohli, A. M. Treviño, C. Massarra, and G. Paulus. 2015. "Cross-Correlation Modeling of European Windstorms: A Cokriging Approach for Optimizing Surface Wind Estimates." *Spatial Statistics* 13: 62–75. doi:10.1016/j.spasta.2015.05.003.

Lee, J. J., and C. H. Kim. 2012. "Roles of Surface Wind, NDVI and Snow Cover in the Recent Changes in Asian Dust Storm Occurrence Frequency." *Atmospheric Environment* 59: 366–375. doi:10.1016/j.atmosenv.2012.05.022.

Liu, Y., J. Stanturf, and S. Goodrick. 2010. "Wildfire Potential Evaluation During a Drought Event with a Regional Climate Model and NDVI." *Ecological Informatics* 5 (5): 418–428. doi:10.1016/j.ecoinf.2010.04.001.

Lloyd, C. D. 2005. "Assessing the Effect of Integrating Elevation Data into the Estimation of Monthly Precipitation in Great Britain." *Journal of Hydrology* 308 (1–4): 128–150. doi:10.1016/j.jhydrol.2004.10.026.

Lorente-Plazas, R., J. P. Montavez, S. Jerez, J. J. Gómez-Navarro, P. Jiménez-Guerrero, and P. A. Jiménez. 2014. "A 49 Year Hindcast of Surface Winds Over the Iberian Peninsula." *International Journal of Climatology published online in Wiley Online Library*. doi:10.1002/joc.4189.

Lorente-Plazas, R., J. P. Montavez, P. A. Jimenez, S. Jerez, J. J. Gomez-Navarro, P. García-Valero, and J. A. Jimenez-Guerrero. 2015. "Characterization of the Surface Wind Over the Iberian Peninsula." *International Journal of Climatology* 35 (6): 1007–1026. doi:10.1002/joc.4034.

Luo, W., M. C. Taylor, and S. R. Parker. 2008. "A Comparison of Spatial Interpolation Methods to Estimate Continuous Wind Speed Surfaces Using Irregularly Distributed Data from England and Wales." *International Journal of Climatology* 28: 947–959. doi:10.1002/joc.1583.

Mentis, D., S. Hermann, M. Howells, M. Welsch, and S. H. Siyal. 2015. "Assessing the Technical Wind Energy Potential in Africa a GIS-Based Approach." *Renewable Energy* 83: 110–125. doi:10.1016/j.renene.2015.03.072.

Morais, R., S. G. Matos, M. A. Fernandes, A. L. G. Valente, S. F. S. P. Soares, P. J .S. G. Ferreira, and M. J. C. S. Reis. 2008. "Reis, Sun, Wind and Water Flow as Energy Supply for Small Stationary Data Acquisition Platforms." *Computers and Electronics in Agriculture* 64 (2): 120–132. doi:10.1016/j.compag.2008.04.005.

Mutua, F., and D. Kuria. 2012. "A Comparison of Spatial Rainfall Estimation Techniques: A Case Study of Nyando River Basin Kenya." *Journal of Agriculture, Science and Technology* 14 (2): 149–165. doi:http://elearning.jkuat.ac.ke/journals/ojs/index.php/jagst/article/view/991/818.

NASA (National Aeronautics and Space Administration). 2015. "ASTER Global Digital Elevation Map." Accessed 10 January 2015. https://asterweb.jpl.nasa.gov/gdem.asp.

Ozelkan, E., S. Bagis, E. C. Ozelkan, B. B. Ustundag, M. Yucel, and C. Ormeci. 2015. "Spatial Interpolation of Climatic Variables Using Land Surface Temperature and Modified Inverse Distance Weighting." *International Journal of Remote Sensing* 36 (4): 1000–1025. doi:10.1080/01431161.2015.1007248.

Ozgonenel, O., and D.V.P. Thomas. 2012. "Short-Term Wind Speed Estimation Based on Weather Data." *Turkish Journal of Electrical Engineering & Computer Sciences* 20 (3): 335–346. doi:10.3906/elk-1012-1.

Patel, M. R. 2006. *Wind and Solar Power Systems: Design, Analysis, and Operation*. 2nd ed. Boca Raton: CRC Press.

Philippopoulos, K., and D. Deligiorgi. 2012. "Application of Artificial Neural Networks for the Spatial Estimation of Wind Speed in a Coastal Region with Complex Topography." *Renewable Energy* 38 (1): 75–82. doi:10.1016/j.renene.2011.07.007.

Sahin, A. D. 2004. "Progress and Recent Trends in Wind Energy." *Progress in Energy and Combustion Science* 30 (5): 501–543. doi:10.1016/j.pecs.2004.04.001.

Schallenberg-Rodriguez, J. 2013. "A Methodological Review to Estimate Techno-Economical Wind Energy Production." *Renewable and Sustainable Energy Reviews* 21: 272–287. doi:10.1016/j.rser.2012.12.032.

Sensoy, S., M. Demircan, Y. Ulupinar, and Z. Balta. 2008. "Turkish State Meteorological Services Report: TürkiyeİklimiClimate of Turkey]." http://www.mgm.gov.tr/FILES/iklim/turkiye_iklimi.pdf.

Sertel, E., S. Kaya, and P. J. Curran. 2007. "Use of Semivariograms to Identify Earthquake Damage in an Urban Area." *IEEE Transactions on Geoscience and Remote Sensing* 45 (6): 1590–1594. doi:10.1109/TGRS.2007.894019.

Sigal, A., M. Cioccale, C. R. Rodríguez, and E. P. M. Leiva. 2015. "Study of the Natural Resource and Economic Feasibility of the Production and Delivery of Wind Hydrogen in the Province of Córdoba, Argentina." *International Journal of Hydrogen Energy* 40 (13): 4413–4425. doi:10.1016/j.ijhydene.2015.01.149.

Thrace Development Agency. 2015. "Thrace Region." Accessed 12 May 2015. http://www.trakyaka.org.tr/content-187-trakya_bolgesi.html.

Tobler, W. 1970. "A Computer Movie Simulating Urban Growth in the Detroit Region." *Economic Geography* 46 (2): 234–240.

Turkish State Meteorological Service. 2003. "Turkish State Meteorological Services Report: Türkiye İklim Sınıflandırması [Turkey Climate Classification]." http://www.mgm.gov.tr/FILES/genel/sss/iklimsiniflandirmalari turkiye.pdf.

UMBC (University of Maryland Baltimore County). 2015. "Department of Geography and Environmental Systems Weather and Climate courses: Chapter 7 – Condensation: Dew, Fog, and Clouds." Accessed 18 May 2015. http://userpages.umbc.edu/~tokay/chapter5new.html.

USGS (United States Geological Survey). 2014 "Earth Explorer." Accessed 15 December 2014. http://earthexplorer.usgs.gov/.

Vahidnia, M. H., A. A. Alesheikh, S. Behzadi, and S. Salehi. 2013. "Modeling the Spread of Spatio-Temporal Phenomena Through the Incorporation of ANFIS and Genetically Controlled Cellular Automata: A Case Study on Forest Fire." *International Journal of Digital Earth* 6 (1): 51–75. doi:10.1080/17538947.2011.603366.

Walker, J. J., K. M. de Beurs, and G. M. Henebry. 2015. "Land Surface Phenology Along Urban to Rural Gradients in the U.S. Great Plains." *Remote Sensing of Environment* 165: 42–52. doi:10.1016/j.rse.2015.04.019.

Wang, J. F., L. F. Li, and G. Christakos. 2009. "Sampling and Kriging Spatial Means: Efficiency and Conditions." *Sensors* 9 (7): 5224–5240. doi:10.3390/s90705224.

Wang, J. F., A. Stein, B. B. Gao, and Y. Ge. 2012. "A Review of Spatial Sampling, Spatial Statistics." *Spatial Statistics* 2: 1–14. 10.1016/j.spasta.2012.08.001.

Yu, M., G. R. Carmichael, T. Zhu, and Y. Cheng. 2012. "Sensitivity of Predicted Pollutant Levels to Urbanization in China." *Atmospheric Environment* 60: 544–554. doi:10.1016/j.atmosenv.2012.06.075.

Zhang, C., W. Li, and D. J. Travis. 2009. "Restoration of Clouded Pixels in Multispectral Remotely Sensed Imagery with Cokriging." *International Journal of Remote Sensing* 30 (9): 2173–2195. doi:10.1080/01431160802549294.